Int. J. Multiphase Flow Vol. 17, No. 2, pp. 159–177, 1991
Printed in Great Britain.

0301-9322/91 $3.00 + 0.00

MEASUREMENT AND PREDICTION OF TRAJECTORIES AND COLLISION OF DROPLETS

Q.-V. NGUYEN, R. H. RANGEL and D. DUNN-RANKIN
Department of Mechanical Engineering, University of California, Irvine, CA 92717, U.S.A.

(Received 25 November 1989; in revised form 17 October 1990)

Abstract—This paper describes a combined experimental and numerical investigation of the interaction effects occurring in a stream of single droplets and small groups of droplets. In particular, we examine the effect of neighboring droplets on droplet drag. The paper has three parts: (1) an analysis of a droplet trajectory utilizing published drag correlations; (2) a comparison of experimental trajectories of single droplets with theoretical trajectories; and (3) an analysis of the droplet–droplet collision that occurs when trailing droplets catch up with the lead droplet. The trailing droplets catch the lead droplet because, residing in the lead droplet's wake, they experience less drag.

Key Words: droplet, drag, vaporization, sprays, streams, interaction

INTRODUCTION

The combustion of liquid fuel droplets occurs in a variety of energy conversion devices. For example, oil-burning power-plant furnaces, gas turbine engines for airplanes, and diesel engines for land transport, all depend on fuel droplet vaporization and combustion for their operation. Even more critically than for energy conversion devices, liquid hazardous waste incinerators require efficient and complete combustion of liquid droplets. A substantial amount of research on the vaporization and burning of isolated droplets has been justified on the basis of such widespread practical application of liquid fuel combustion [for example, see reviews by Law (1982) and Sirignano (1983)]. In practical devices, however, liquid fuel actually enters the combustion chamber as a spray, not as a collection of isolated droplets. In a spray, the presence of neighboring droplets invalidates many isolated droplet assumptions. Despite the distinct difference between sprays and isolated droplets, present combustion models simply characterize a spray as a summation of isolated droplets, letting a "correction factor" account for the influence of neighboring droplets. A recent workshop on combustion of sprays and droplets (Sanders & Bergan 1989) suggests that these numerical models are currently inadequate in part because droplet–droplet interactions are not included properly. To help address this inadequacy, this work uses a continuous stream of droplet packets to examine the effect of droplet–droplet interactions on droplet trajectory.

Numerical simulation is often an integral part of the combustor design process, and consequently, the accuracy of the numerical model determines how well a "paper" combustor actually performs once it is constructed. Substantial benefits derive, therefore, from improved numerical simulation of the combustion process. In the area of spray combustion, improving numerical simulations is difficult because processes occurring on the scale of droplet sizes (100–200 μm) control the operation of practical devices with an overall length scale on the order of meters (Sirignano 1986). Computationally resolving such diverse scales is impractical, necessitating the use of simplified submodels for the small-scale controlling processes. Present simplified submodels derive entirely from single-droplet quasi-steady droplet theory, and they do not, therefore, properly account for droplet interaction. An eventual benefit of the current work is the improvement of these submodels to adequately address the interacting droplet phenomena that may control spray combustion.

This paper includes both experiments and analyses of droplet trajectories. In the experiments we measure the trajectories of individual droplets, droplet pairs, droplet triples and droplet quadruples. We then compare these measured trajectories with trajectories predicted by solving the equation of motion for the droplets. Each solution of the equation of motion includes different laws for droplet drag and droplet vaporization. The comparison between the experiments and the analyses

helps determine the importance of droplet–droplet interaction and the validity of the different drag and vaporization laws.

LITERATURE REVIEW OF RELATED RESEARCH

Numerical Studies

Existing numerical models (e.g. El Banhawy & Whitelaw 1980; Raju & Sirignano 1987a) for the comprehensive solution of large-scale spray combustion flows are limited to a cost-effective computational grid that cannot resolve controlling phenomena occurring on the scale of the droplet size. Developments at the other end of the resolution spectrum include complete and accurate models for the unsteady axisymmetric behavior of a single vaporizing or burning droplet (Patnaik *et al.* 1986; Dwyer & Sanders 1988a,b). In calculations involving a large number of droplets in a gas flow, however, such detailed computations are prohibitively expensive.

In practice, simplified versions of the high-resolution comprehensive models help bridge the gap between single-droplet calculations and complete combustor design calculations. Unfortunately, however, the simplified versions of the comprehensive models do not properly account for the effects of neighboring droplets. Neighboring droplets, in particular, affect droplet vaporization and droplet drag.

Droplet vaporization

Labowsky (1980) presented an analysis of particle interaction in a quiescent gas and found that the vaporization rate depends on the array geometry. Labowsky (1980) found that for a three-particle array, with inter-droplet spacing of five droplet radii, the vaporization rate decreases to 72% of the isolated droplet vaporization rate. Other analyses of droplet vaporization in quiescent atmospheres produced results similar to those of Labowsky (Twardus & Brzustowski 1977; Umemura *et al.* 1981).

Global studies of vaporization and combustion of large droplet clouds have also been presented (Chiu *et al.* 1982; Correa & Sichel 1982; Bellan & Harstad 1987a, b). These global models cannot address, however, the processes occurring on the scale of the droplet size. Global models, therefore, rely on the accuracy of droplet submodels for the calculation of vaporization rates.

Droplet drag

Droplet drag calculations that account for both the Stefan flow, and for the influence of neighboring droplets are inconclusive. Consequently, modelers usually use values of the drag coefficient corresponding to a solid sphere, with a correction for the effect of vaporization. The effect of neighboring droplets on droplet drag has received attention only recently (Raju & Sirignano 1987b, 1989; Chiang & Sirignano 1990). Results of these numerical studies suggest that neighboring droplets affect the droplet drag significantly.

Experimental Studies

Similar to numerical studies, experimental investigations of droplet vaporization usually consist of full-spray investigations or single-droplet studies. Experiments involving a small group of droplets are rare. In addition, the few experimental results available in the literature that describe small groups of droplets address vaporization only; the effects of neighboring droplets on droplet drag are not discussed.

Droplet vaporization

Nuruzzaman *et al.* (1971) examined monosized droplet streams in stationary flames, and found that the vaporization rate decreased to approximately one-half the isolated droplet value. In this study the inter-droplet spacing was relatively large (approx. 30 droplet diameters). Miyasaka & Law (1981) showed that, in agreement with theoretical predictions, interacting droplets do not vaporize with the classic d^2 law of isolated droplets. The effect of buoyancy on the vaporization process was also affected substantially by the presence of neighboring droplets. These droplets were suspended on filaments and were quite large (1 mm with 5 mm spacing). Because the droplets were

suspended, the influences of droplet motion were not included in the study. Twardus & Brzustowski (1978) made qualitative measurements of flame spread through arrays of freely-falling burning droplets. Again the droplet size was large (2.5 mm with a spacing of 55 mm). The vaporization rate and the drag were not measured, only the flame speed. Sangiovanni & Kesten (1976) presented a study of combustion in monodispersed droplet streams, but they were concerned primarily with ignition criteria, and consequently they did not report inidividual droplet behavior in detail.

THEORETICAL MODEL FOR PREDICTING DROPLET TRAJECTORY

Equations of Motion

Our theoretical model uses a simplified analysis of the equations describing the motion of a vaporizing droplet. In these calculations, the droplet and the air form an isothermal system. We neglect the effect of the droplet on the surrounding air. The air is at rest, and has uniform and constant temperature. There is no buildup of the vaporizing species. With these assumptions, only the droplet trajectory and momentum equations need to be solved:

$$\frac{d\mathbf{x}}{dt} = \mathbf{v}, \qquad \frac{d\mathbf{v}}{dt} = \mathbf{g} - \frac{C_D}{2}\frac{\rho R^2}{m} v\mathbf{v}, \tag{1}$$

where $\mathbf{x}$ and $\mathbf{v}$ are the droplet position and velocity vectors, respectively, v is the magnitude of the velocity vector, $\mathbf{g}$ is the gravity vector, t is time, C_D is the drag coefficient, ρ is the air density, R is the droplet radius and m is the droplet mass. We neglect virtual mass and buoyancy effects.

For a vaporizing droplet the droplet size varies with time:

$$\frac{4}{3}\pi\rho_L \frac{dR^3}{dt} = -\dot{m}, \tag{2}$$

where ρ_L is the liquid density. Solution of this equation requires a model for the vaporization rate, $\dot{m}$. In addition, the droplet momentum equation, [1], requires a model for the drag coefficient. In this analysis we compare the predicted trajectory of a droplet using various available correlations for the drag coefficient and the vaporization rate. The predicted values are then compared with experimental trajectories. Based on this comparison we will eventually modify the correlations to account for interaction effects between droplets.

Drag Coefficient Models

The drag coefficient is

$$C_D = \frac{D}{\frac{1}{2}\rho v^2 \pi R^2}, \tag{3}$$

where D is the magnitude of the drag force acting on the droplet. Most drag coefficient correlations used in the combustion literature account for a Reynolds number effect and a vaporization effect through a dependence on the transfer number B. No correlation for the drag coefficient accounting for the combined dependence on the Reynolds and transfer numbers as well as on droplet–droplet interaction is available in the literature, although the work of Raju & Sirignano (1989) and Chiang & Sirignano (1990) may produce correlations for two droplets in tandem. Some common single-droplet correlations are described below.

Stokes drag

The Stokes drag correlation (Stokes 1851) is strictly valid for a solid sphere at $\mathrm{Re} < 1$. It is included because its use yields an analytical solution to the trajectory equations. This analytical solution gives physical insight into the parameters controlling the droplet trajectory. The Stokes drag coefficient is given by

$$C_D = \frac{24}{\mathrm{Re}}, \tag{4}$$

where the Reynolds number is defined by $\mathrm{Re} = 2Rv\rho/\mu$. Equation [4] yields the Stokes-drag formula, $D = 6\pi\mu Rv$, for the force acting on a sphere.

Solid sphere drag

Yuen & Chen (1976) experimentally showed that for low to moderate vaporization rates ($B = c_p(T_\infty - T_s)/h_{fG} \leqslant 3$) the drag coefficient of an evaporating droplet may be approximated by the standard drag curve for a solid sphere, provided the gas viscosity μ is evaluated at a reference temperature and the concentration obtained by using the 1/3-rule:

$$T_{ref} = T_s + \tfrac{1}{3}(T_\infty - T_s), \qquad Y_{F,ref} = Y_{Fs} + \tfrac{1}{3}(Y_{F\infty} - Y_{Fs}). \tag{5}$$

Yuen & Chen (1976) argue that the decrease in viscous drag due to blowing is accompanied by an increase in the pressure drag of similar magnitude. The solid sphere drag curve is approximated within 10% by the curve-fit formula (White 1974):

$$C_D = \frac{24}{Re} + \frac{6}{1 + Re^{0.5}} + 0.4, \tag{6}$$

in the range $0 \leqslant Re \leqslant 2 \times 10^5$. However, the solid sphere correlation is invalid for high vaporization rates and for droplets with wake flames (Sirignano 1983).

Renksizbulut–Yuen drag

Renksizbulut & Yuen (1983a) conducted numerical experiments with droplets in air streams up to 1059 K, and, comparing their results with the experimental data of Yuen & Chen (1976) and Eisenklam *et al.* (1967), proposed the following correlation for the drag coefficient:

$$C_D = \frac{24}{Re}(1 + 0.2\,Re^{0.63})(1 + B)^{-0.2}, \tag{7}$$

for $10 < Re < 300$. In this equation, all thermophysical properties are evaluated using the mean between the surface and ambient values of the temperature and mass fraction; the density in Re, however, is based on the free-stream value. The $(1 + B)^{0.2}$ factor accounts for the reduction in drag due to the blowing effect of evaporation.

Chiang et al. drag

Chiang *et al.* (1991) propose the following drag correlation, which agrees within 4% with results from their variable-property Navier–Stokes numerical calculations:

$$C_D = \frac{24}{Re}(1 + 0.41\,Re^{0.405})(1 + B)^{-0.32}, \tag{8}$$

for $30 < Re < 250$, $0.6 < B < 6$. The thermophysical properties are evaluated as in the Renksizbulut–Yuen correlation. The Chiang *et al.* correlation indicates a larger reduction in drag due to blowing than does the Renksizbulut–Yuen correlation.

Vaporization Models

Most vaporization models employ the classical d^2 law for vaporization with a correction for convective effects. For large Re, a vaporization model based on a flat-plate boundary-layer analogy may also be reasonable (Sirignano 1978).

Classical theory: d^2 law

Quasi-steady theory (Spalding 1953) assumes that the rate of surface regression of the droplet is negligible, an assumption that is valid for very large droplets and porous spheres. When the thermophysical properties and the surface and ambient fuel mass fractions are constant, quasi-steady theory yields a d^2 law for the variation of the droplet size. The vaporization rate is given by

$$\dot{m} = 4\pi R \rho \mathscr{D} C_{Re} \ln(1 + B_M), \tag{9}$$

where $\mathscr{D}$ is the mass diffusivity of the gas, $B_M = (Y_{Fs} - Y_{F\infty})/(1 - Y_{Fs})$ is the mass transfer number, and C_{Re} is the correction which accounts for convective effects. Two commonly used correlations for the convective correction are the Ranz & Marshall (1952) correlation,

$$C_{Re} = 1 + 0.3\,Re^{0.5}Sc^{0.333}, \tag{10}$$

with Sc as the Schmidt number; and the Clift *et al.* (1978) correlation,

$$C_{Re} = \tfrac{1}{2}[1 + (1 + ReSc)^{0.333} f(Re)], \quad [11]$$

where $f(Re) = 1$ for $Re \leqslant 1$ and $f(Re) = Re^{0.077}$ for $1 < Re < 400$ and $0.25 < Sc < 100$. This correlation approximates numerical results from various sources with 3% error.

Abramzon–Sirignano model

Abramzon–Sirignano (1989) provide a correlation which agrees with the classical theory in the limit of very small Re but which replaces the $\ln(1 + B)$ dependence with an exponential law for high Re. The exponential law allows the vaporization to agree with the experimental data of Renksizbulut & Yuen (1983b).The vaporization rate is

$$\dot{m} = 4\pi R\rho\mathscr{D}\left[1 + \frac{C_{Re} - 1}{F(B)}\right]\ln(1 + B_M), \quad [12]$$

where

$$F(B) = (1 + B_M)^{0.7}\frac{\ln(1 + B_M)}{B}. \quad [13]$$

All thermophysical properties are evaluated with the 1/3-rule, except for the density appearing in the Re which is evaluated at the free-stream value. The $1/n$-rule indicates that a property P is evaluated at the reference condition $P_{ref} = [(n - 1)P_s + P_\infty]/n$, with subscript s representing the surface and subscript ∞ representing the free stream.

Renksizbulut–Yuen model

Based on experiments, Renksizbulut & Yuen (1983b) provided a correlation for the Nusselt number of a droplet evaporating in air:

$$Nu = (2 + 0.57\,Re^{0.5}Pr^{0.333})(1 + B_T)^{-0.7}, \quad [14]$$

where the 1/2-rule is used to evaluate the thermophysical properties, except for the density in the Re which is the free-stream density. This correlation is valid for $10 < Re < 2000$. Renksizbulut & Haywood (1988) provide an expression for the vaporization rate as

$$\dot{m} = 4\pi R\rho\mathscr{D}\frac{Nu}{2}B_T, \quad [15]$$

where Nu is given by [14] and the transfer number $B_T = c_p(T_\infty - T_s)/h'_{fG}$ takes into account the heat transferred into the droplet.

Chiang–Sirignano model

From numerical calculations, Chiang & Sirignano (1990) have reported Sherwood and Nusselt number correlations equivalent to those of Renksizbulut & Yuen. They do not provide an expression for the vaporization rate. However, by analogy with the Abramzon–Sirignano model, the vaporization rate is

$$\dot{m} = 4\pi R\rho\mathscr{D}\frac{Sh}{2}B_M, \quad [16]$$

where the Sherwood number Sh is

$$Sh = (2 + 0.46\,Re^{0.6}Sc^{0.333})(1 + B_M)^{-0.7} \quad [17]$$

valid for $0.3 < B_M < 4.5$ and $30 < Re < 250$.

TRAJECTORY ANALYSIS

For an isolated droplet, [1] and [2] can be solved to predict the droplet trajectory for a given set of initial conditions, and for specific droplet drag and vaporization models. In our calculations,

the droplets are released from a height h_0 with a horizontal initial velocity V_{x0}. The initial vertical velocity is zero.

Analytical Solution of Droplet Trajectory

In the simplified case of a constant temperature, non-vaporizing droplet experiencing Stokes drag, [1] can be solved analytically to obtain the position and velocity of the droplet:

$$x = V_{x0}\tau\left[1 - \exp\left(-\frac{t}{\tau}\right)\right] \qquad [18]$$

and

$$y = h_0 + g\tau^2\left[1 - \exp\left(-\frac{t}{\tau}\right)\right] - g\tau t. \qquad [19]$$

The parameter $\tau = m/6\pi\mu R$ is a characteristic time of droplet deceleration and corresponds to the ratio of the initial droplet momentum mV_{x0} over the initial Stokes drag force $6\pi\mu V_{x0}R$. For a 50 μm dia droplet in room air, τ is approx. 6 ms. The velocity components are

$$V_x = V_{x0}\exp\left(-\frac{t}{\tau}\right) \qquad [20]$$

and

$$V_y = g\tau\left[\exp\left(-\frac{t}{\tau}\right) - 1\right], \qquad [21]$$

and the droplet trajectory is obtained by combining [18] and [19] to eliminate time:

$$y = 1 + \frac{g\tau}{V_{x0}h_0}x - \frac{g\tau^2}{h_0}\ln\left(\frac{1}{1 - \dfrac{x}{\tau V_{x0}}}\right). \qquad [22]$$

Defining the dimensionless distances $\tilde{x} = x/(\tau V_{x0})$ and $\tilde{y} = y/h_0$, [22] can be written as

$$\tilde{y} = \tilde{g}\left[\tilde{x} - \ln\left(\frac{1}{1-\tilde{x}}\right)\right], \qquad [23]$$

where the parameter $\tilde{g} = g\tau^2/h_0$ is a dimensionless gravity representing a ratio of characteristic heights. Equation [18] shows that $\tilde{x} \to 1$ asymptotically. Hence, the maximum x position is proportional to $V_{x0}R^2$. A droplet twice as large will travel 4 times as far.

With the same non-dimensionalization, the parabolic ballistic trajectory is

$$\tilde{y} = -\tfrac{1}{2}\tilde{g}\tilde{x}^2, \qquad [24]$$

which follows directly from [23] in the limit $\tilde{x} \ll 1$ with $\tau\tilde{x}$ finite. Figure 1 compares trajectories predicted by [23] and [24] for the case of $\tilde{g} = 0.0063$, which corresponds to a 50 μm dia droplet traveling in room air with $h_0 = 10$ cm and $V_{x0} = 1$ m/s.

From the trajectories we can also determine how the separation distance between two droplets injected in tandem varies with time. Raju & Sirignano (1989) and Chiang & Sirignano (1990) compute the separation using detailed Navier–Stokes calculations. Here we assume that the Stokes drag formula applies and we neglect interaction effects. Two droplets are injected at times $t = 0$ and $t = t_0$, respectively. In the following subscript 1 refers to the lead droplet, and subscript 2 refers to the trailing droplet. The dimensionless separation between these droplets at any time greater than t_0 is $\Delta r = [(V_{x0}\tau\,\Delta\tilde{x})^2 + (h_0\,\Delta\tilde{y})^2]^{0.5}$, where

$$\Delta\tilde{x} = \tilde{x}_1 - \tilde{x}_2 = \exp(-\tilde{t})[\exp(-\tilde{t}_0) - 1], \qquad \Delta\tilde{y} = \tilde{y}_1 - \tilde{y}_2 = \tilde{g}\exp(-\tilde{t})[\exp(\tilde{t}_0) - 1] - \tilde{g}\tilde{t}_0, \qquad [25]$$

where $\tilde{t} = t/\tau$ is the dimensionless time. The horizontal separation decreases monotonically from its initial value of $1 - \exp(-t_0)$ to zero, while the vertical separation increases monotonically from its initial value of $\tilde{g}[\exp(-\tilde{t}_0) - 1 + \tilde{t}_0]$ to an asymptotic value of $\tilde{g}\tilde{t}_0$.

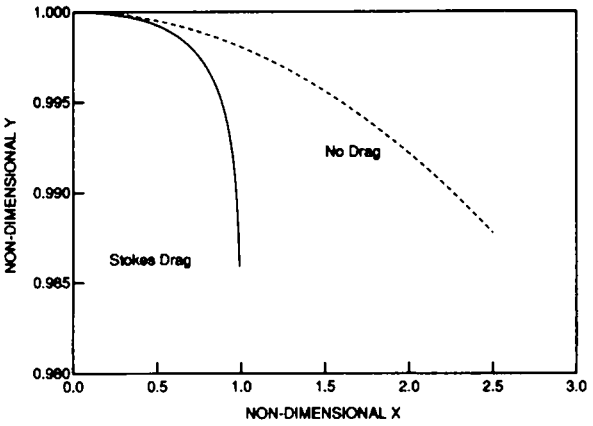

Figure 1. Trajectories in room temperature air for non-vaporizing 50 μm dia spheres with and without a Stokes drag force. Initial velocity = 1 m/s; initial height = 10 cm; sphere density = 760 kg/m^3.

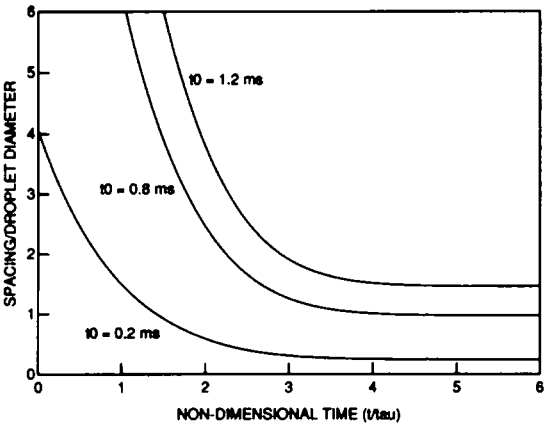

Figure 2. Spacing between two spheres injected at the same velocity but separated by lag time t_0. The spheres are non-vaporizing, and experience only Stokes drag. The calculation is for two 50 μm dia spheres in room temperature air. The initial velocity of the spheres is 1 m/s and their density is 760 kg/m^3. Collision occurs when the spacing/droplet diameter falls below 1.

To determine the possibility of droplet collision, it is useful to calculate the ratio of the separation distance to the droplet diameter $\Delta\tilde{r} = \Delta r/2R$. When this quantity is equal to one, the two droplets are in contact. The square of this ratio is

$$\Delta\tilde{r}^2 = \frac{V_{x0}^2\tau^2}{4R^2}\exp(-2\tilde{t})[\exp(\tilde{t}_0) - 1]^2 + \frac{g^2\tau^4}{4R^2}\{\exp(-\tilde{t})[\exp(\tilde{t}_0) - 1] - \tilde{t}_0\}^2. \quad [26]$$

As this equation indicates, the dimensionless separation between droplets asymptotes to the value $\Delta\tilde{r}_\infty = g\tau t_0/(2R)$ for large time. This separation is only in the vertical direction. A collision occurs when $\Delta\tilde{r} = 1$. To avoid a collision, injection of the second droplet must be made after a time lag t_0:

$$t_0 = \frac{2R}{g\tau}. \quad [27]$$

For two 50 μm dia droplets injected at 1 m/s, the time lag must be >0.81 ms, which corresponds to an initial horizontal spacing of $\Delta\tilde{x} = 0.12$ or 760 μm (15 diameters) from center to center. It is interesting that the necessary time lag depends only on the drop size, as $t_0 \propto 1/R$. Larger drops require less time lag. The condition on t_0 is necessary but not sufficient to avoid a collision. The separation may go through a minimum before increasing to its asymptotic value. However, this occurs only in cases with low initial velocity. Figure 2 shows the time variation of the dimensionless separation $\Delta\tilde{r}$ for different values of the initial time lag, $\tilde{t}_0$.

Numerical Solution of Droplet Trajectory

The previous analysis does not apply for a vaporizing droplet or for a droplet with an Re > 1. For these cases, we use a numerical solution of [1] and [2] after prescribing a drag coefficient model and a vaporization model from those listed earlier. We integrate [1] and [2] using an implicit Runge–Kutta scheme. The calculations terminate when the droplet mass is 1% of the initial mass.

Figure 3(a) shows the predicted droplet trajectories using various drag coefficient models for a 100 μm dia droplet of methanol, with an initial velocity of 10 m/s in air at 300 K. For these calculations, the Abramzon–Sirignano vaporization model is used. Most drag coefficient models predict a similar trajectory, but the Stokes drag formula gives a much longer trajectory because of the drag's lower dependence on velocity. The Chiang–Sirignano model predicts a slightly lower drag because of a stronger effect of the transfer number. This lower drag increases the maximum horizontal travel, and gives a higher curvature to the droplet trajectory. The Chiang–Sirignano drag correlation, however, is valid only for Re > 30, and the droplets in our experiments are out of this range in a short time.

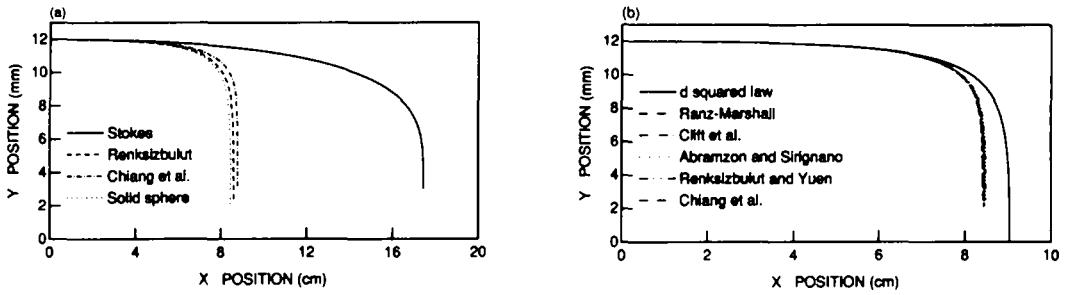

Figure 3. The effect on the calculated droplet trajectory in room temperature air of (a) various drag models and (b) various vaporization models. The droplets have an initial diameter of 50 μm and an initial velocity of 10 m/s.

A comparison of various vaporization models is shown in figure 3(b). Here we use the drag coefficient for a solid sphere. Except for the classical d^2 model, all of the vaporization models produce nearly the same droplet trajectory in room temperature air. In room air, therefore, the droplet trajectory is insensitive to the vaporization model.

EXPERIMENTS

Experimental Apparatus

The experimental apparatus is shown in figure 4, and consists of a droplet generator, a droplet charging/deflection system, a droplet velocimeter and a photographic imaging system. The entire apparatus, excluding the flow system and electronics are mounted on an optical breadboard. An aluminum-framed Plexiglas enclosure ($0.76 \times 0.76 \times 0.61$ m) covers the apparatus to prevent external air currents from disrupting the droplet trajectory. Further details of the experimental apparatus are described by Nguyen *et al.* (1989).

Droplet generator

The droplet generator is similar to that described by Berglund & Liu (1973). Bottled nitrogen from a regulator pressurizes methanol contained in a reservoir. The pressurized methanol jets through a 40 μm orifice. A piezoelectric crystal oscillates the orifice as the jet issues from it. The oscillation breaks the methanol jet into uniform droplets at the frequency that is driving the crystal. We drive the crystal with a square wave from a function generator amplified with an audio power amplifier. We typically drive the crystal with a ± 50 V square wave at 12–20 kHz.

Droplet deflection system

We use an electronic droplet charging/deflection system similar to that described by Russo *et al.* (1981) and Sangiovanni & Kesten (1976) to produce widely spaced droplets and droplet groups. A medium voltage pulse (250 V) selectively charges droplets negatively as they detach from the jet of liquid near the orifice. A -7 kV potential across two copper plates then deflects the charged droplets. We produce sequential droplet packets by not-charging small groups of drops. A razor blade separates the deflected drops from the undeflected drops, allowing the undeflected, uncharged droplets to pass into the measurement region.

A signal derived by digitally dividing the function generator output that drives the piezoelectric crystal controls the production of droplet packets, generating a continuous sequence of isolated droplets or droplet groups.

Droplet velocimeter

The droplet velocity was computed by measuring the droplet transit time between two single-mode optical fibers (4 μm core) epoxied together with a separation of 250 μm. We place the fibers approx. 1 mm from the droplet trajectory. Helium–neon laser light transmitted through the fibers produces two distinct sources of light. The droplets scatter the light to a photomultiplier tube

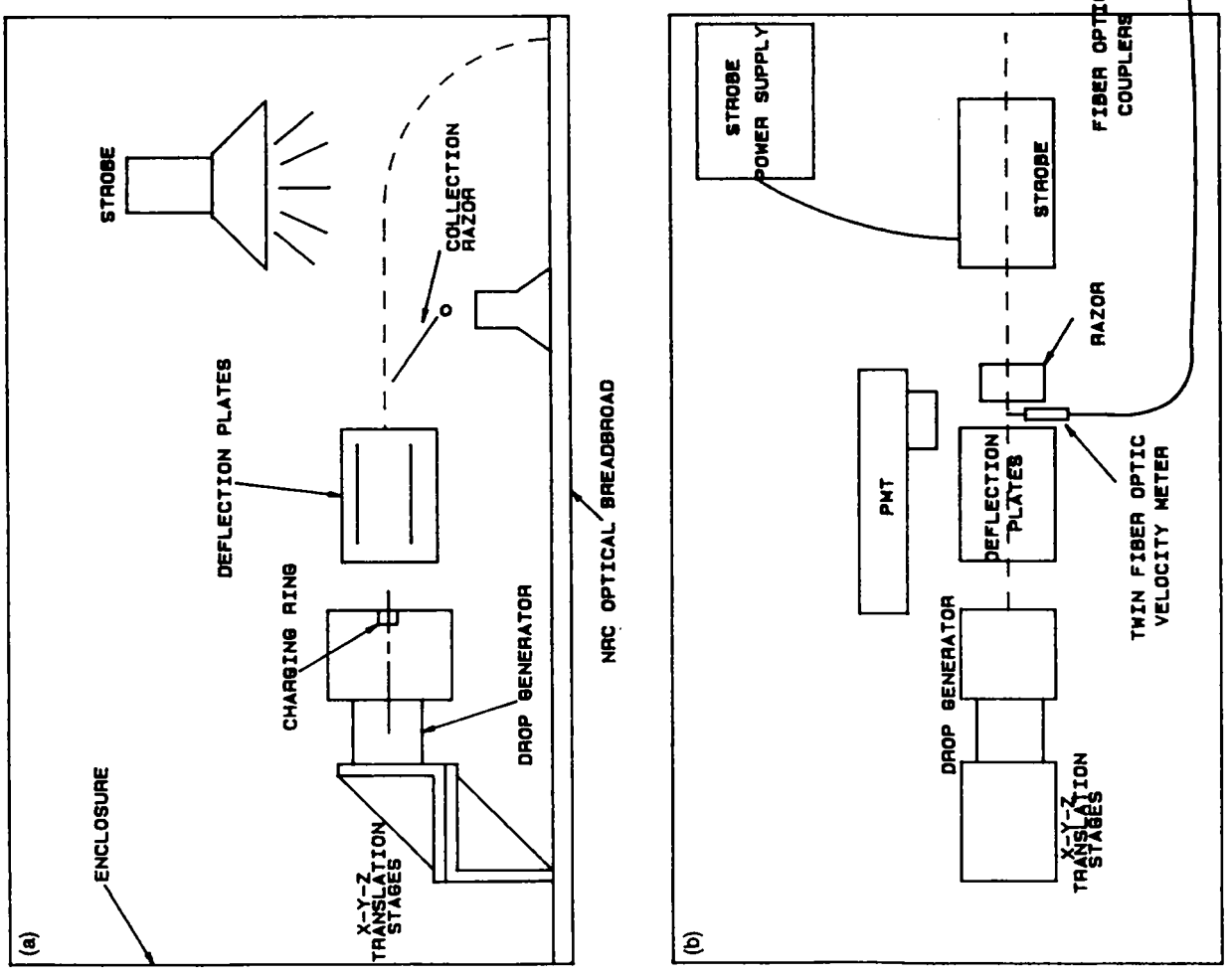

Figure 4. Schematic of the experimental apparatus: (a) side view; and (b) top view.

as they pass. The signal from the PMT is then recorded on an oscilloscope, with the temporal spacing of the pulses providing a transit time for velocity determination. The uncertainty in velocity from the transit time measurement is approx. 5%.

We also use the light pulses from the twin-fiber velocimeter to detect the uniformity of the droplet stream, to determine the number of droplets in a packet, the droplet spacing within a packet and the spacing between droplets.

Photographic system

Once the droplet packets are generated, we record their trajectory on Kodak TRI-X film using a 35 mm SLR camera equipped with a macro lens. For the detailed collision data we use a video camera mounted to a stereo microscope. A xenon flash lamp above the droplet stream illuminates the trajectory. The strobe is synchronized to the packet generation pulses, and consequently provides a stroboscopic image of the droplet trajectory. The camera shutter is open for about 2 s to allow sufficient exposure time. Since there is a continuous sequence of droplets, the multiple exposures map out the entire droplet trajectory in a single image.

To measure droplet size, we photograph the droplet stream through a stereo microscope. For size measurements, we backlight the droplets with a single strobe from the xenon flash lamp to capture individual droplets. We corroborate the droplet size measurements by using a precision micrometer to translate reticle cross-hairs across the droplet image in the stereo microscope during an experiment. The uncertainty in droplet size is approx. 5%.

Experimental Procedure

The first step is to establish a uniform and stable stream of droplets. This is done by adjusting the piezoelectric crystal driving frequency and amplitude while monitoring the laser light being scattered from the stream. When a stable and clean trace is observed on the oscilloscope, the stream is monodisperse. At this point, we record the frequency, and we measure the droplet size. We then adjust the charging pulse width, amplitude and delay for maximum deflection between charged and uncharged droplets.

Once a reasonable amount of deflection is obtained, the next step is to get isolated drop groups. We switch the drop charging unit to a packet generation mode. In this mode, the charging unit prevents a fixed number of drops from being charged. The digital divide circuit controls the rate at which a packet of drops is not charged. The packet length is then adjusted until the desired droplet packet is observed on the oscilloscope trace. With reliable droplet packets available, we record the time spacing between the leading and trailing droplet, and the spacing between droplet groups. We then photograph the trajectory.

We extract the information on the photographic film by projecting the negative with a slide projector onto a sheet of graph paper. The enlargement ratio is carefully adjusted to match the calibrated film plane distance, and we trace the trajectory onto the graph paper manually. We use a graphics plotter to digitize the manual tracing. The data is then ready for comparison with theoretical calculations.

EXPERIMENTAL RESULTS AND DISCUSSION

The experimental results include both droplet trajectories and droplet collisions. The droplet collisions occur because droplets in the wake of a lead droplet experience less drag, and consequently catch up and coalesce with the lead droplet. In these experiments, this collision and coalescence occurs so early after the droplets separate from the primary droplet stream that the droplet trajectory is essentially that of a single coalesced droplet. Analyzing these droplet trajectories provides a relationship between the drag coefficient and the droplet Re. The first subsection describes trajectories of single droplets; the second subsection extracts the drag coefficient from the trajectory data; and the third subsection details the collision process.

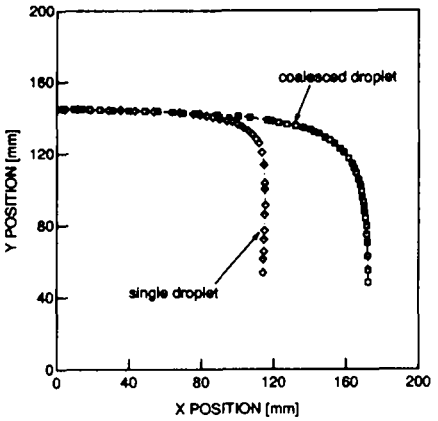

Figure 5. Experimental droplet trajectories for (a) a single droplet and (b) a coalesced droplet.

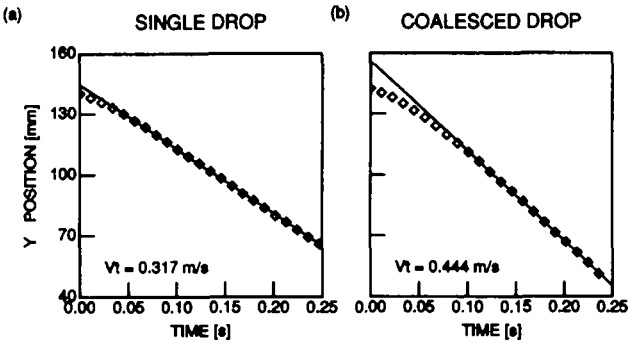

Figure 6. Stroboscopic record of the y position as a function of time near the knee of the droplet trajectory for (a) a single droplet and (b) a coalesced droplet. There is 0.011 s between data points. The slope of the least-squares fit line gives the terminal velocity.

Droplet Trajectories

Predicting droplet trajectories

Figure 5 shows the trajectories of two streams of droplets. One stream consists of single primary droplets, and the other stream contains larger droplets formed by the coalescence of a droplet pair. The trajectories in figure 5 are digitized from long-time exposure photographs of the two droplet streams. Based on the fluid flow rate and the droplet generation frequency, the primary droplet size is approx. 128 μm. Doubling the mass of a primary droplet gives the coalesced droplet diameter as 161 μm. From the fiber optic velocimeter, the initial velocity of the single droplets is 6.42 m/s, and the initial velocity of the coalesced droplets is 6.79 m/s. The initial time spacing between droplets in both streams is 11.2 ms, which is equivalent to a horizontal spacing of approx. 76 mm (472 coalesced droplet diameters). With such wide separation, there is negligible interaction between droplets.

The long-term exposure data provides the droplet trajectory, x vs y, but cannot furnish $x(t)$ or $y(t)$ information. By synchronizing a flash lamp to the droplet packet generation, however, a stroboscopic photograph of the droplet streams provides $x(t)$ and $y(t)$ at discrete time intervals. Figure 6 shows $y(t)$ near the knee of the droplet trajectories shown in figure 5. Time zero in figure 6 is arbitrary and corresponds approximately to an x position of 80 mm in figure 5. For both the single drop and the coalesced drop, the y position is a linear function of time after 0.1 s, indicating that the droplets have reached a terminal velocity. A linear least-squares fit to $y(t)$ after 0.1 s indicates terminal velocities of 0.317 and 0.444 m/s for the single and coalesced droplets, respectively. Since vaporizing droplets do not achieve terminal velocity, these results suggest that droplet vaporization is negligibly small in this experiment. Figure 7 relates the measured terminal velocity to droplet size by using the drag correlations described earlier. The variation between correlations is small but significant, particularly for the smaller droplet. Part of the discrepancy occurs because the correlations are not valid at the Re corresponding to the terminal velocity. The terminal Re for both droplets is <5, and only the solid sphere correlation is recommended ($\mathrm{Re} < 10$). The droplet sizes from the solid sphere correlation are 132 and 165 μm for the single and coalesced droplets, respectively. These droplet diameters are nearly equal to the initial droplet diameters determined from the fluid flow rate and droplet generation frequency, indicating that the droplets do not vaporize in this experiment. Evidently, the continuous droplet stream generates a saturated vapor tunnel that prevents droplet vaporization.

Figure 8 compares the measured droplet trajectories to calculated trajectories using the solid sphere correlation for the droplet drag. The initial droplet velocity comes from the velocimeter measurements. The terminal velocity measurements determine the droplet size. The calculation assumes a saturated vapor environment that suppresses vaporization. The calculation over predicts by $<5\%$ the maximum x value for both the single and coalesced droplets. Further, with less than a 5% decrease in the initial velocity (which is within experimental uncertainty) the agreement

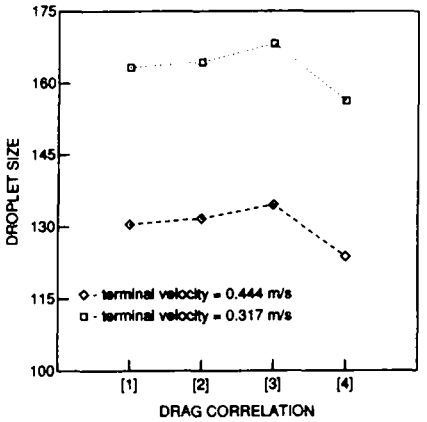

Figure 7. Droplet size computed from the terminal velocity based on various drag laws: [1] Yuen & Chen (1976); [2] Renksizbulut & Yuen (1983a,b); solid sphere, Chiang *et al.* (1991).

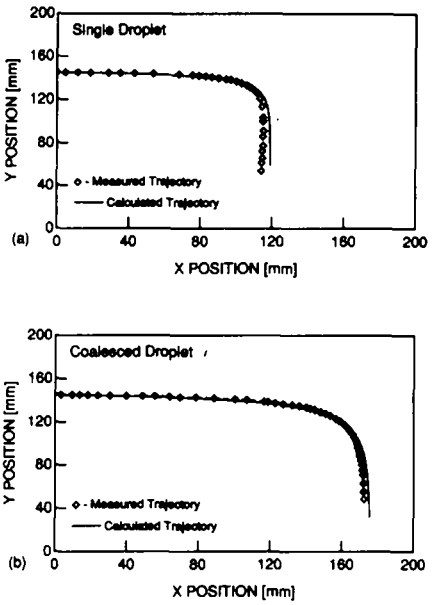

Figure 8. Comparison between measured droplet trajectories and computed trajectories for (a) a single droplet and (b) a coalesced droplet. The computed trajectories use the solid sphere drag law.

between calculation and measurement is nearly perfect. These results indicate that the solid sphere drag model for individual non-vaporizing droplets provides reliable prediction of droplet trajectory.

Predicting $x(t)$ and $y(t)$ data is a more stringent test of drag correlations than is predicting the trajectory. Figure 9 shows a stroboscopic $x(t)$ data at the knee of the droplet trajectory. This data corresponds to the $y(t)$ data in figure 6. The linear coefficient of a least squares cubic fit to the

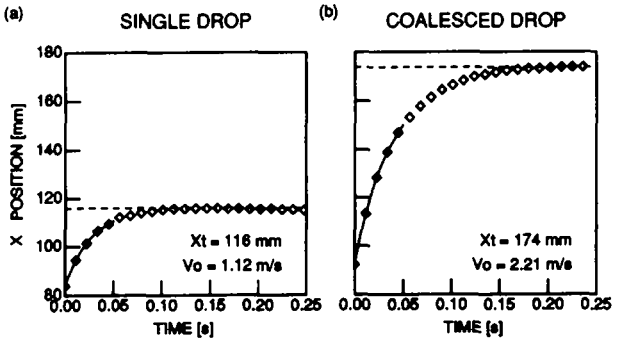

Figure 9. Stroboscopic record of the x position as a function of time near the knee of the droplet trajectory for (a) a single droplet and (b) a coalesced droplet. There is 0.011 s between data points. The initial velocity and terminal x position are indicated in the figures.

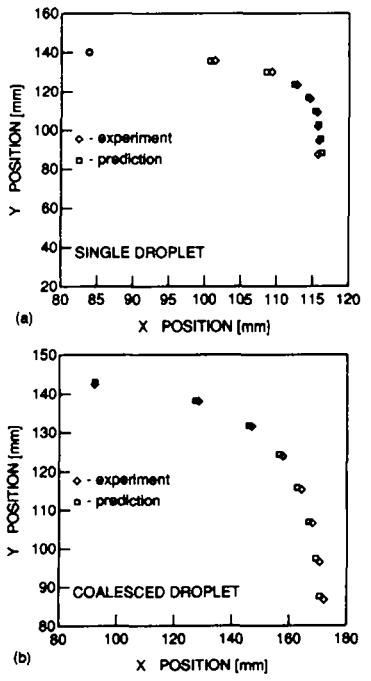

Figure 10. Comparison between measured and computed stroboscopic records of the droplet trajectories for (a) a single droplet and (b) a coalesced droplet. There is 0.011 s between data points, and the calculated trajectory uses the solid sphere drag model.

first 5 points on each $x(t)$ curve provides an initial velocity, and the droplet size is assumed from the terminal velocity results. Figure 10 compares x–y positions calculated with these initial conditions with measured x–y positions at fixed instants in time. The calculations assume solid sphere drag and no vaporization. In figure 10, the prediction lags the measurement slightly, but the agreement is very good. As with the trajectories, nearly perfect agreement can be achieved with only slight modifications (within experimental uncertainty) of the droplet size and initial velocity.

Determining the Drag Coefficient

By differentiating the $x(t)$ and $y(t)$ data from the stroboscopic photographs, it is possible to extract a relationship between the drag coefficient C_D and Re. In fact, the $x(t)$ and $y(t)$ data provide independent determinations of C_D to verify the reliability of this relationship.

Typically, drag coefficients are extracted from position data by fitting a polynomial to the data and then differentiating the polynomial. For our trajectories, however, polynomial functions are unreasonable because they do not have the correct physical behavior at long times. Specifically, $x(t)$ must asymptote to a limiting x value as $t \to \infty$, and $\dot{y}(t)$ must asymptote to a terminal velocity as $t \to \infty$. Polynomials can provide neither of these features. Consequently, we fit our data with exponential functions.

Drag coefficient from x(t)

The $x(t)$ function should asymptote to a terminal x position, suggesting a function of the form

$$x(t) = x_\infty + b\, e^{-ct}, \qquad [28]$$

with x_∞ representing the terminal x value; $x_\infty + b$ is the initial x value. Differentiating [28] with time gives $\dot{x}(t) = -bc\, e^{-ct}$. Hence $-bc$ is the initial velocity. The initial and terminal x, and the initial velocity, define the exponential function precisely. Unfortunately, extracting the initial velocity from the data is difficult and inexact. Consequently, the best exponential fit to the data requires some manipulation of $-bc$. Figures 11(a,b) show exponential fits to the $x(t)$ data with bc adjusted to give the fit with minimum deviation from the data.

The drag coefficient for x is defined as

$$C_{Dx} = \frac{-ma_x}{\frac{1}{2}\rho V V_x A}, \qquad [29]$$

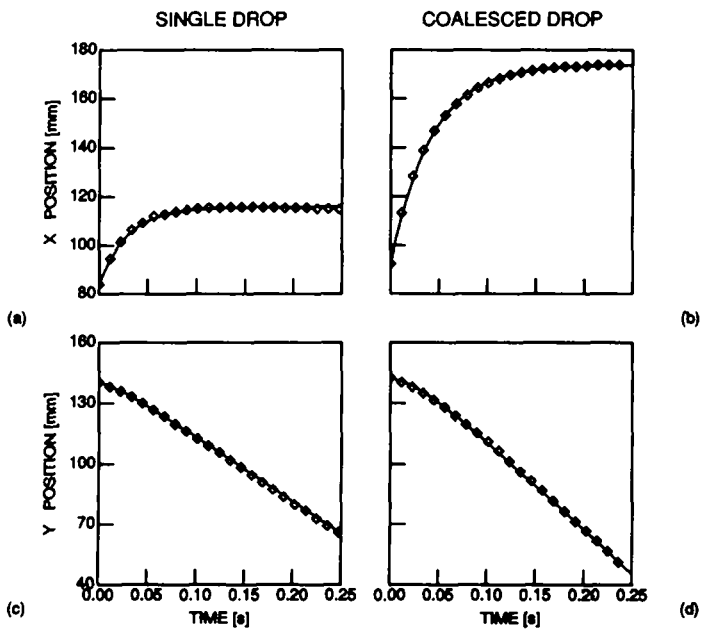

Figure 11. Exponential fits to stroboscopic records of $x(t)$ and $y(t)$ to be used for calculating the drag coefficient.

where m is the droplet mass, a_x is the droplet acceleration in the x direction, ρ is the gas density, V_x is the speed in the x direction, V is the magnitude of the total velocity, $\sqrt{V_x^2 + V_y^2}$, and A is the droplet projected area. Simplifying:

$$C_{Dx} = -\frac{8}{3}\frac{\rho_L}{\rho}\frac{Ra_x}{VV_x}, \quad [30]$$

with ρ_L the droplet density and R the droplet radius. Adding viscosity μ and rearranging:

$$C_{Dx} = -\left(\frac{8\rho_L R^2}{3\mu}\right)\left(\frac{\mu}{\rho VR}\right)\left(\frac{a_x}{V_x}\right), \quad [31]$$

which for constant drop radius, drop density, and viscosity, can be written as

$$C_{Dx} = -\left(\frac{K}{Re}\right)\left(\frac{a_x}{V_x}\right) \quad [32]$$

with K a constant. For the exponential form of [28], a_x/V_x is simply equal to the coefficient $-c$, and $C_{Dx} = \text{const/Re}$. While this form of C_D is not robust enough to span a large Re range, it is reasonable over small ranges, and is exact for the Stokes flow regime, $Re < 0.5$.

Drag coefficient from y(t)

The $y(t)$ function should provide a terminal velocity, so V_y should asymptote to a constant value. An exponential function with this behavior is

$$y(t) = V_t t + b + c\,e^{-dt}, \quad [33]$$

where V_t is the terminal velocity, $b + c$ is the initial y value and $V_t - dc$ is the initial velocity. A fourth equation comes from assigning a fixed $y(t_*)$ somewhere on the curve. These four conditions define the $y(t)$ function completely. As with the $x(t)$ function, uncertainties in the positions and velocities require some adjustment of the parameters to give a good fit to all of the data. Figures 11(c,d) show the functions fit to the $y(t)$ data that give minimal deviation from the data. Because of the linear term in $y(t)$, C_{Dy} is not simply related to Re as is C_{Dx}:

$$C_{Dy} = -\left(\frac{K}{Re}\right)\left(\frac{a_y}{V_y}\right) \quad [34]$$

and

$$C_{Dy} = -\left(\frac{K}{Re}\right)\left(\frac{d^2c\,e^{-dt}}{V_t - dc\,e^{-dt}}\right). \quad [35]$$

As $t \to \infty$, $C_{Dy} \to \text{const/Re}$, which is the correct form of C_D in Stokes flow. Figure 12 compares the drag coefficient computed from both the single and coalesced droplet and from both $x(t)$ and $y(t)$ data. The solid curve is the solid sphere correlation. Except for C_{Dy} of the coalesced droplet at $Re > 10$, all of the results are very close to the solid sphere correlation.

Droplet Collision

Our earlier Stokes analysis predicts that successive droplets with the same initial velocity will collide if their initial spacing is less than some critical value. Figure 13 shows high resolution measurements of $x(t)$ for droplet pairs, triples and quadruples. All droplets are 128 μm dia. The initial droplet spacing within a droplet packet is 850 μm at the packet generation point, and the corresponding initial velocity is 12 m/s. The figure gives the x position for the lead droplet and for each trailing droplet. In all cases the droplets collide and coalesce into a single large droplet. It is difficult to observe the collision in figure 13 because the droplet spacing is a small fraction of the droplet travel distance. Figure 14 provides the droplet positions relative to the lead drop for each case. While there is some curvature in the relative position data, the spacing decreases approximately linearly with time for all trailing droplets. Further, the average approach velocity is nearly the same for the first, second and third trailing drop as evidenced by the fact that all lines are parallel. The spacing between successive trailing droplets is approximately constant, and they approach the lead drop as a group. This result indicates that the influence of a wake diminishes

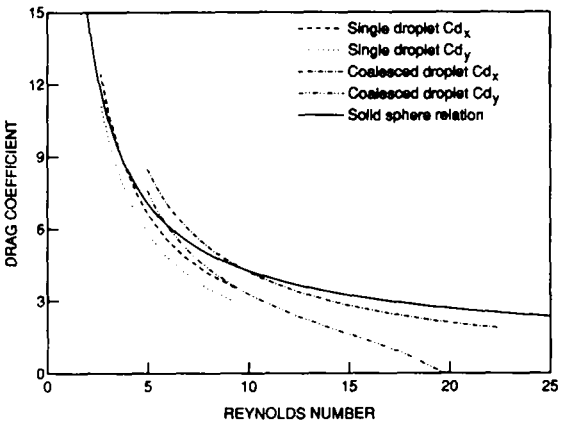

Figure 12. Drag coefficient calculated from exponential fits to the $x(t)$ and $y(t)$ stroboscopic records for both a single droplet and a coalesced droplet.

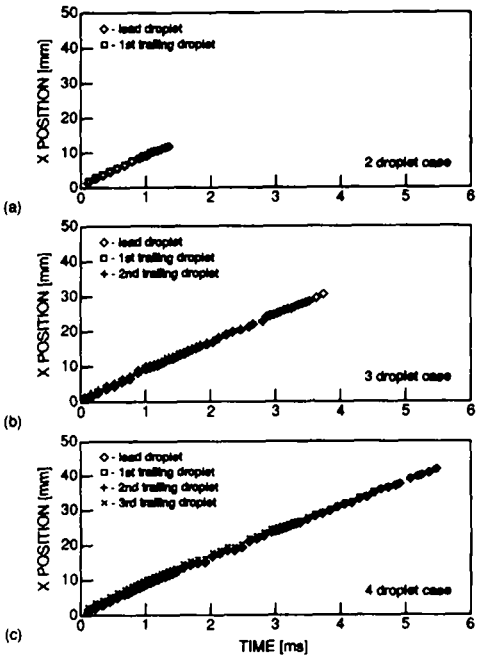

Figure 13. Detailed x position as a function of time before droplet coalescence for (a) a 2-droplet group, (b) a 3-droplet group and (c) a 4-droplet group.

significantly from the first trailing drop to the succeeding trailing drops, a result noted in the numerical work of Tal *et al.* (1983).

There are distinct breaks at approx. 1.5 and 3.5 ms in the 3- and 4-drop spacing results of figure 14. These breaks coincide with the coalescence of a trailing droplet with the lead droplet. While the spacing decreases approximately linearly with time, careful analysis of the spacing between coalescence events reveals curvature, which indicates a relative acceleration between the lead droplet and the trailing drops. This difference in acceleration is caused by reduced drag on the trailing droplets. Unfortunately, the largest drag difference occurs just as the droplet packets are formed inside the deflection plates of the experimental apparatus. This location is currently inaccessible for measurement. The drag difference from the packet generation point to the initial measurement point produces the velocity difference of approx. 0.30 m/s between the lead and trailing droplets that is represented by the slope of the data in figure 14. This velocity difference is much larger than the velocity difference occurring because of the small time lag between droplets, indicating that the rear droplet experiences less drag than the lead droplet. Because of the scatter in the data it is difficult to extract reliable drag differences from the data in figure 14. However, a qualitative analysis can indicate the relative drag between the lead and trailing droplets. For one-dimensional acceleration of equal mass droplets, the ratio of the lead droplet drag to the first trailing droplet drag in terms of the relative droplet acceleration is

$$\frac{Fd_t}{Fd_l} = 1 - \frac{\ddot{x}_r}{\ddot{x}_l}, \qquad [36]$$

where subscripts l, t and r refer to lead, trail and relative, respectively. This result means that if $x_r(t)$ and $x_l(t)$ have curvature in the same direction, the drag on the trailing drop is less than that on the lead droplet. Figure 15(a) shows the droplet spacing between the lead droplet and the first trailing droplet. The curves are least-square parabolic fits to the data, making the tacit assumption that the relative acceleration a_r is constant over the measurement. The data is somewhat scattered, but all of the parabolas are concave down, indicating negative relative acceleration. Figure 15(b) shows the lead droplet position x_l as a function of time. Again the curves are least-square parabolic fits to the data. All of these curves are also concave down, indicating that the trailing droplet experiences less drag than does the lead droplet. The ratio of drag force Fd_t/Fd_l from these parabolic fits are: (1) 2-drop case—0.93; (2) 3-drop case—0.17; and (3) 4-drop case—0.78. The 3-drop case

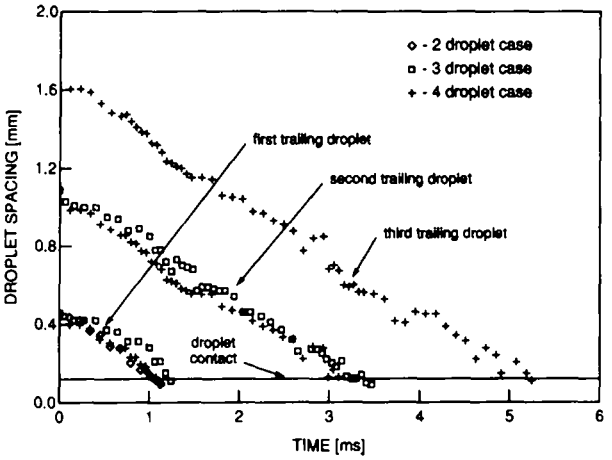

Figure 14. Droplet spacing as a function of time between trailing droplets and the lead droplet for 2-, 3- and 4-droplet groups. Collision occurs when droplets cross the "droplet contact" line.

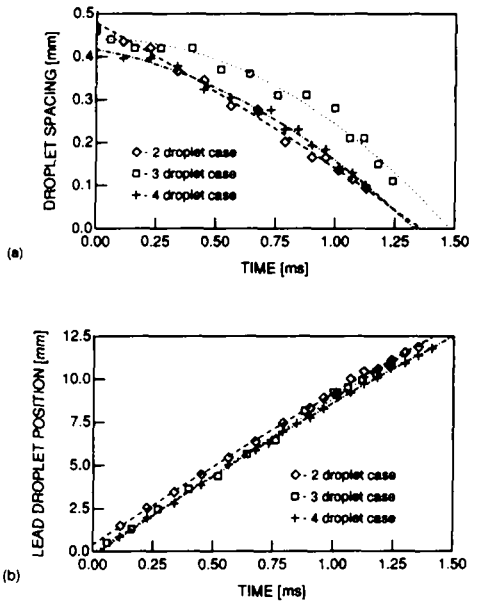

Figure 15. Detailed droplet behavior for 2-, 3- and 4-droplet groups showing (a) droplet spacing between the first trailing drop and the lead drop and (b) the position of the lead droplet. The curvature of these data indicate the relative acceleration between the lead and trailing droplets.

is significantly different from the other two cases because of the high curvature of the droplet spacing, indicating very high relative acceleration. Unfortunately, the data from the 3-drop case has more scatter than the other two cases and is therefore less reliable.

Another technique to estimate the drag difference between the lead and trailing droplet is to use the droplet drag models verified in the trajectory section above. We can reduce the drag on the trailing droplet until the measured difference velocity of 0.30 m/s is obtained over the 30 mm distance from the deflection plates to the first measurement point. A linear least-squares fit to the first 10 points in figure 15(b) provides a lead droplet velocity at the first measurement point of 8.7 m/s. We use the drag model to predict the initial velocity at the packet generation point that gives 8.7 m/s at the first measurement point. Using the solid sphere drag model in this process, the average drag ratio of the trail to leading droplet that produces a 0.3 m/s difference is approx. 0.9. Furthermore, this result is insensitive to the value chosen for the initial velocity at the packet generation point. The drag reduction of 0.9 agrees fairly well with the 2- and 4-drop fitting analysis above, and indicates that 3-drop case result is unreasonably low. The average drag reduction of 0.9 is valid only for the 7-drop diameter initial droplet spacing of these experiments. For comparison, numerical computations by Tal *et al.* (1983) indicate a drag reduction of 0.70 for droplet triples with a droplet spacing of 1.5 dia, and Liu *et al.* (1988) demonstrate drag reductions of <0.2 for a continuous droplet stream relative to isolated droplets.

CONCLUSIONS

This work compares experimentally determined trajectories of droplets with trajectories predicted by using various vaporization and drag laws in the equation of motion. The predictions, experiments and their comparison lead to the following conclusions for droplet trajectories and drag under our experimental conditions:

1. While the inclusion of droplet vaporization affects the theoretical droplet trajectory significantly, at room temperature conditions there is little influence of the specific vaporization law chosen from among those in the literature.
2. All of the drag correlations examined, even when used outside their recommended Re range, give similar results for the droplet trajectory. The correlation of Chiang

et al. (1991) gives slightly lower drag than the other correlations. Because the Re is outside the Stokes regime for most of the droplet's horizontal flight, the Stokes drag law predicts much lower drag than the correlation drag formulas.

3. Under the room temperature conditions of our experiments, isolated droplets do not vaporize. Droplets in a continuous droplet stream, even when separated by several hundred droplet diameters, produce a saturated vapor tunnel that prevents droplet vaporization.
4. For non-vaporizing droplets, experimental single-droplet trajectories match the predicted single droplet trajectories extremely well (within 5%).
5. Exponential fits to the trajectory data provide the proper limit behaviors: (a) a terminal x position; and (b) a terminal y velocity. The relationship between Re and the drag coefficient, calculated from exponential fits to the trajectory data, agrees reasonably well with the solid sphere drag correlation, particularly at low Re. However, because the drag coefficient requires twice differentiating position data, the results are sensitive to the curve-fitting procedure. By comparing drag coefficients calculated from $x(t)$ data with those calculated from $y(t)$ data, we find good consistency in our results for low Re.
6. Trailing droplets closely separated from a lead droplet catch up and collide with the lead droplet in a very short time. The collision occurs because the trailing droplets experience reduced drag in the wake of the lead droplet. The drag reduction is approximately the same for all trailing droplets regardless of their position in the sequence. All trailing droplets behave similarly, moving to catch the lead droplet as a group. They do not catch up with their nearest leading neighbor until that neighbor is the lead drop of the group.
7. Under the conditions of our experiments, our measurements and calculations indicate that the trailing droplets experience a drag reduction of approx. 10% compared with the drag of the lead droplet. This drag reduction causes droplet collision for 130 μm droplets initially separated by 1 mm to occur in approx. 3 ms.

Acknowledgements—This work was supported, in part, by the Universitywide Energy Research Group of the University of California and by the National Science Foundation. We also acknowledge the assistance in the laboratory of Mr Tao Sun.

REFERENCES

ABRAMZON, B. & SIRIGNANO, W. A. 1989 Droplet vaporization model for spray combustion calculations. *Int. J. Heat Mass Transfer* **32,** 1605–1618.

BELLAN, J. & HARSTAD, K. 1987a Analysis of the convective evaporation of non dilute clusters of drops. *Int. J. Heat Mass Transfer* **30,** 125–136.

BELLAN, J. & HARSTAD, K. 1987b Ignition of non dilute clusters of drops in convective flows. *Combust. Sci. Technol.* **53,** 75–87.

BERGLUND, R. N. & LIU, B. Y. H. 1973 Generation of monodisperse aerosol standards. *Envir. Sci. Technol.* **7,** 147–153.

CHIANG, C.-H. & SIRIGNANO, W. A. 1990 Numerical analysis of convecting and interacting vaporizing fuel droplets with variable properties. Presented at the *28th AIAA Aerospace Sciences Mtg*, Reno, Nev.

CHIANG, C.-H., RAJU, M. S. & SIRIGNANO, W. A. 1991 Numerical analysis of convecting, vaporizing fuel droplets with variable properties. *Int. J. Heat Mass Transfer.* To be published.

CHIU, H. H., KIM, H. Y. & CROKE, E. J. 1982 Internal group combustion of liquid droplets. In *Proc. 19th Symp. (Int.) on Combustion*, pp. 971–980. The combustion Institute, Pittsburgh, Pa.

CLIFT, R., GRACE, J. R. & WEBER, M. E. 1978 *Bubbles, Drops, and Particles.* Academic Press, New York.

CORREA, S. M. & SICHEL, M. 1982 The group combustion of a spherical cloud of monodisperse fuel droplets. In *Proc. 19th Symp. (Int.) on Combustion*, pp. 981–991. The Combustion Institute, Pittsburgh, Pa.

DWYER, H. A. & SANDERS, B. R. 1988a Fuel droplets. In *Proc. 21st Symp. (Int.) on Combustion*, pp. 633–639. The Combustion Institute, Pittsburgh, Pa.

DWYER, H. A. & SANDERS, B. R. 1988b Unsteady influences in droplet dynamics and combustion. *Combust. Sci. Technol.* **58,** 253.

EISENKLAM, P., ARUNACHALAM, S. A. & WESTON, J. A. 1967 Evaporation rates and drag resistance of burning drops. In *Proc. 11th Symp. (Int.) Symp. on Combustion*, pp. 715–728. Butterworths, London.

EL BANHAWY, Y. & WHITELAW, J. H. 1980 Calculation of the flow properties of a confined kerosene-spray flame. *AIAA Jl* **18,** 1503–1510.

LABOWSKY, M. 1980 Calculation of the burning rates and interacting fuel droplets. *Combust. Sci. Technol.* **22,** 217–226.

LAW, C. K. 1982 Recent advances in droplet vaporization and combustion. *Prog. Energy Combust. Sci.* **8,** 171–201.

LIU, D. Y., ANDERS, K. & FROHN, A. 1988 Drag coefficients of single droplets moving in an infinite droplet chain on the axis of a tube. *Int. J. Multiphase Flow* **14,** 217–232.

MIYASAKA, K. & LAW, C. K. 1981 Combustion of strongly-interacting linear droplet arrays. In *Proc. 18th Symp. (Int.) on Combustion*, pp. 283–292. The Combustion Institute, Pittsburgh, Pa.

NGUYEN, Q.-V., RANGEL, R. H. & DUNN-RANKIN, D. 1989 Measurement and prediction of trajectories for vaporizing droplet pairs. Presented at the *Western States Section/The Combustion Institute Fall Mtg*, Sandia National Labs, Livermore, Calif., Paper 89-12.

NURUZZAMAN, A. S. M., HEDLEY, A. B. & BEÉR, J. M. 1971 Combustion of monosized droplet streams in stationary self-supporting flames. In *Proc. 13th Symp. (Int.) on Combustion*, pp. 787–799. The Combustion Institute, Pittsburgh, Pa.

PATNAIK, G., SIRIGNANO, W. A., DWYER, H. A. & SANDERS, B. R. 1986 A numerical technique for the solution of a vaporizing fuel droplet. *Prog. Astronaut. Aeronaut.* **105,** 253.

RAJU, M. S. & SIRIGNANO, W. A. 1987a Spray computations in centerbody combustor. *Proc. 2nd ASME–JSME therm. Engng Joint Conf.* **1,** 61–71.

RAJU, M. S. & SIRIGNANO, W. A. 1987b Unsteady Navier–Stokes solution for two interacting vaporizing droplets. Presented at the *AIAA 25th Aerospace Sciences Mtg*, Reno, Nev.

RAJU, M. S. & SIRIGNANO, W. A. 1989 Interaction between two vaporizing droplets in an intermediate Reynolds number flow. *Phys. Fluids.*

RANZ, W. E. & MARSHALL, W. R. 1952 Evaporation from drops. *Chem. Engng Prog.* **48,** 141–173.

RENKSIZBULUT, M. & HAYWOOD, R. J. 1988 Transient droplet evaporation with variable properties and internal circulation at intermediate Reynolds numbers. *Int. J. Multiphase Flow* **14,** 189–202.

RENKSIZBULUT, M. & YUEN, M. C. 1983a Numerical study of droplet evaporation in a high-temperature stream. *J. Heat Transfer* **105,** 389–397.

RENKSIZBULUT, M. & YUEN, M. C. 1983b Experimental study of droplet evaporation in a high-temperature air stream. *J. Heat Transfer* **105,** 384–388.

RUSSO, R. E., WITHNELL, R. & HIEFTJE, G. M. 1981 Simple and inexpensive design for an isolated droplet generator useful for studies of atomization in flames. *Appl. Spectrosc.* **35,** 531–536.

SANDERS, B. R. & BERGAN, N. E. 1989 Workshop on mass, momentum, and energy exchange in combusting sprays: droplet studies. Sandia National Labs Technical Report SAND89-8442.

SANGIOVANNI, J. J. & KESTEN, A. S. 1976 Effect of droplet interaction on ignition in monodispersed droplet streams. In *Proc. 16th Symp. (Int.) on Combustion*, pp. 577–592. The Combustion Institute, Pittsburgh, Pa.

SIRIGNANO, W. A. 1978 Theory of multicomponent fuel droplet vaporization. *Archwm Termodynam. Spalan.* **9,** 231–247.

SIRIGNANO, W. A. 1983 Fuel droplet vaporization and spray combustion theory. *Prog. Energy Combust. Sci.* **9,** 291–322.

SIRIGNANO, W. A. 1986 The formulation of spray combustion models: resolution compared to droplet spacing. *J. Heat Transfer* **108,** 633–639.

SPALDING, D. B. 1953 The combustion of liquid fuels. In *Proc. 4th Symp. (Int.) on Combustion*, pp. 847–864. Williams & Wilkins, Baltimore Md.

STOKES, G. G. 1851 On the effect of internal friction of fluids on the motion of pendulums. *Trans. Camb. philos. Soc.* **9,** 8–106.

TAL, R., LEE, D. N. & SIRIGNANO, W. A. 1983 Hydrodynamics and heat transfer in sphere assemblages—cylindrical cell models. *Int. J. Heat Mass Transfer* **26,** 1265–1273.

TWARDUS, E. M. & BRZUSTOWSKI, T. A. 1977 The interaction between two burning fuel droplets. *Archwm Termodynam. Spalan.* **8,** 347–358.

TWARDUS, E. M. & BRZUSTOWSKI, T. A. 1978 An experimental study of flame spread and burning in arrays of monosize hydrocarbon droplets. *Combust. Sci. Technol.* **17,** 215–225.

UMEMURA, A., OGAWA, S. & OSHIMA, N. 1981 Analysis of the interaction between two burning droplets. *Combust. Flame* **41,** 45–55.

WHITE, F. M. 1974 *Viscous Fluid Flow*, p. 209. McGraw-Hill, New York.

YUEN, M. C. & CHEN, L. W. 1976 On drag of evaporating liquid droplets. *Combust. Sci. Technol.* **14,** 144–154.